Available online at www.sciencedirect.com
ScienceDirect
Thin Solid Films 515 (2007) 4826–4833
thin solid films
www.elsevier.com/locate/tsf

Characteristic curves of hydrogenated amorphous silicon based solar cells modeled with the defect pool model

E. Klimovsky [a], A. Sturiale [b], F.A. Rubinelli [b,*]

[a] *Facultad Regional Paraná, Universidad Tecnológica Nacional, Almafuerte 1033, 3100, Paraná Entre Ríos, Argentina*
[b] *INTEC, Universidad Nacional del Litoral, Güemes 3450, 3000, Santa Fe, Argentina*

Received 31 August 2006; received in revised form 20 November 2006; accepted 6 December 2006
Available online 19 January 2007

Abstract

Using the improved expression of the defect pool model proposed by Powell and Deane we match the experimental current–voltage and the spectral response characteristic curves of hydrogenated amorphous silicon solar cells. We compare the electrical parameters resulting from using the different defect pool models published in the literature and from assuming a uniform density of dangling bond in every device layer. We discuss the applicability of the algorithm derived by Schumm for the stabilized state exploring its sensitivity to the sample history. Finally we propose an expression for stabilized cells adapting Schumm's ideas to the expression derived by Powell and Deane.

PACS codes: 73.61.J; 84.60.J; 73.40
Keywords: Amorphous materials; Silicon; Solar cells

1. Introduction

Hydrogenated amorphous silicon (a-Si:H will be abbreviated as a-Si) thin films are currently used in solar cells and numerous electronic devices. The low processing temperatures and the large area manufacturability facilitate the cost-effective production of solar cells. Intrinsic plasma deposited a-Si prepared by Plasma Enhanced Chemical Vapor Deposition (PECVD) can be considered as device quality material when properties like the dark conductivity, the photoconductivity, the optical gap, the mid-gap electronic density of states (DB), the absorption coefficient, etc., meet pre-established criteria [1]. The a-Si density of states (DOS) consists of parabolic conduction (CB) and valence bands (VB) (extended states) that exponentially decay inside the gap into the conduction band tail (CBT) and valence band tail (VBT) respectively and of mid-gap states (DB) that are usually described by three Gaussian distributions containing amphoteric states recognized as D^+, D^0 and D^-. It was a common practice in the past two decades to assume the presence of a uniform density of DB (UDM) on the whole a-Si intrinsic layer of a-Si based solar cells [2–4] and to adopt a higher density of DB in the stabilized state than in the initial state [4,5]. The Gaussian distribution of DB does not contain information about the origin of these states. Nonuniform densities of DB in the intrinsic layer of a-Si solar cells were also proposed by few authors with some success [6,7]. The defect pool model (DPM), taking shape in the beginning of the nineties [8–11], suggested that DB result from the conversion of Si–Si weak-bonds (WB) (WB ↔ DB) through chemical-type reactions involving DB, Si–Si WB, and Si–H bonds. The equilibrium state distribution of DB resulting from minimizing the entropy of this system appropriately described the defect structure in doped and undoped a-Si in thermal equilibrium as well as the metastable defect formation under non-equilibrium [7,9]. The Si–Si WB distribution is associated with the VB tail [12]:

$$G_D(E) = G_{DO}\exp(-E/E_{DO}) \quad (1)$$

where E_{DO} is the VBT slope, E is the gap state energy referred to the valence band edge and G_{DO} is the density of states value at the valence band edge. The distribution of available defect

* Corresponding author. Tel.: +54 342 4559175; fax: +54 342 4550944.
E-mail address: pancho@ceride.gov.ar (F.A. Rubinelli).

0040-6090/$ - see front matter © 2006 Elsevier B.V. All rights reserved.
doi:10.1016/j.tsf.2006.12.126

sites $P(E)$ where DB are created, or defect pool, is described by the Gaussian distribution:

$$P(E) = \frac{1}{\sqrt{2\pi}\sigma_{DP}} \quad \exp \quad \left[-\frac{(E-E_{DP})^2}{2\sigma_{DP}^2}\right] \tag{2}$$

where σ_{DP} is the standard deviation of the pool and E_{DP} is the peak or pool center (or the most probable DB energy). Powell and Deane derived this expression for the DB density [9]:

$$N_{DB}(E) = \gamma\left[\frac{2}{F_{EQ}^0(E)}\right]^{\frac{\rho kT_{FR}}{E_{DO}}} P\left[E + \frac{\rho\sigma_{DP}^2}{E_{DO}}\right] \tag{3}$$

where F_{EQ}^0 is the equilibrium occupation of neutral DB states and E_{DO} is the VBT slope. The scaling factor γ is given by a complex expression and ρ can be expressed as [9]:

$$\rho = 2E_{DO}/(2E_{DO} + ikT_{FR}) \tag{4}$$

where i indicates the number of Si–H bonds mediating in the WB ↔ DB reaction. This number could be 0, 1, or 2. The pool width σ_{DP} is not a free input parameter and it can be extracted from the following expression [9]:

$$\Delta = \frac{2\cdot\rho\cdot\sigma_{DP}^2}{E_D(T_{FR})} - U = E_{D^+} - E_{D^-}^* \tag{5}$$

where Δ is the separation between the non-occupied D^+ peak (E_{D^+}) and the double occupied D^- peak (E_{D^-}*, where E_{D^-}* = E_{D^-} U). The neutrality condition in (i)-a-Si leads us to the relationship $E_{DP}=E_F+\Delta$ / 2, where E_F is the Fermi level. Hence we have that $E_{DP}\sim E_{D^+}$. The factor γ and the expressions (3)–(5) are not identical in the other versions of the defect pool model published in the literature [9–11]. The dependence of F_{EQ}^0 with respect to the Fermi level in Eq. (3) gives rise to highly non-uniform density of DB along the intrinsic layer of a p–i–n a-Si structure with a higher DB density near the interfaces than in the bulk. The DB distribution profile is evaluated in the solar cell at the freeze-in temperature T_{FR} (which is higher than the device operational temperature T). The temperature dependence of the VBT slope is accounted by [13]:

$$E_{VO}^2(T) = E_{VO}^2(T=0) + kT^2. \tag{6}$$

Powell–Deane published two different algorithms of the DPM [9,10] that we will recognize as DPM1 (Eqs. (1)–(5)) and DPM2 and Schumm proposed one expression for the initial state and other for the stabilized state that we will recognize as DPM3 and DPM4 respectively [11].

In previous publications we showed that although the experimental current–voltage (J–V) and spectral response (SR) characteristic curves of a-Si and a-SiGe p–i–n based solar cells could be matched by adopting either the UDM or the DPM approach only the implementation of the DPM allowed us to achieve higher efficiencies in a-Si and a-SiGe p–i–n solar cells when gap grading in the intrinsic layer was performed [14,15]. Particularly in a-SiGe p–i–n cells the use of the UDM did not allow us to justify the gap grading regularly performed in the intrinsic layer [16]. Using the DPM we found that the optimum band gap profile should have an exponential shape decreasing from the interfaces towards the intrinsic layer bulk [17]. A careful experimental analysis provided by the Rutherford Backscattering Technique confirmed our predictions [18]. In a-Si p–i–n solar cells we could fit the dark J–V curve in a p-i-n cell with a 500 nm thick i-layer and the light J–V in cells with 215, 500, and 1000 nm thick i-layers [15] using the UDM and different versions of the DPM. However we could not fit the same characteristic curves when two Si–H were participating in the WB ↔ DB reaction (i=2), the option most widely accepted by the scientific community because this reaction has the highest probability and the uppermost entropy [9–11,19–21]. We predicted that the efficiency of the a-Si p–i–n solar cell could also be improved by grading the gap and the boron concentration in the intrinsic layer following a similar approach as the described in a-SiGe solar cells [15].

In this paper we describe in detail the procedure followed to match the experimental a-Si solar cell characteristic curves and we compare the resulting electrical parameter values obtained with the UDM and with the different versions of the DPM. We discuss the difficulties associated to the use of the defect pool model in a-Si solar cell modeling. Finally we propose the improved algorithm of Powell and Deane (DPM2) as the best choice to model a-Si solar cells and we discuss how to overcome the bottle-necks that appear in the initial state and in the stabilized state.

2. Experimental details

Samples were grown by PECVD and characterized at Utrecht University, the Netherlands. The solar cells were deposited in the super-strate configuration: SnO_2/p-a-SiC:H/i-a-Si:H/n-a-Si:H/Ag. The intrinsic layer thickness was 215, 500, or 1000 nm thick. Three thin layers (0.5 nm) with decreasing content of carbon were included between the p- and the intrinsic layer. The total density of DB (5×10^{15} cm^{-3}) and the Urbach tail (48 meV) were extracted with the Constant Photocurrent Measurement technique. The activation energies of doped layers were obtained from temperature dependence of the dark conductivity as 0.47 eV and 0.24 eV in the p-, and n-layer respectively. To reach the stabilized state samples were light-soaked with a white light of 100 mW cm^{-2} intensity at controlled temperature ($T\sim$45 °C) during 3000 h and under open circuit conditions.

3. Modeling

Our simulations were performed with the computer code D-AMPS [22] where trapping and recombination terms were conveniently modified to include the DPM. The hydrogen concentration [H] was fixed to 3.5×10^{21} cm^{-3}. The freezing temperature was initially set to 500 K following the work published by Powell and Deane [9,11]. The correlation energy U was assumed equal to 0.2 eV [9–11]. The most probable energy E_{DP} was adopted equal to the peak of the D^+ Gaussian resulting from fitting solar cell characteristics with the UDM and subsequently changed but keeping the activation energy

Table 1
List of electrical input parameters resulting from fitting the *J–V* and SR curves of an a-Si based *p–i–n* solar cell with a 500 nm thick *i*-layer using the UDM

Parameters	(*p*) a-SiC	(*i*) a-Si initial	(*i*) a-Si stabilized	(*n*)a-Si
W (nm)	7	500	500	20
E_G (eV)	2.00	1.72	1.72	1.76
N_c, N_v (cm^{-3})	2×10^{20}	2×10^{20}	2×10^{20}	2×10^{20}
μ_N(cm^2V^{-1} s^{-1})	10	20	20	20
μ_P (cm^2 V^{-1} s^{-1})	1	3.5	3.5	2
E_D (meV)	80	50	50	50
E_A (meV)	45	30	30	30
t_N^+, t_P^- (cm^2)	1×10^{-14}	9.0×10^{-15}	1.5×10^{-14}	1×10^{-15}
t_N^0, t_P^0 (cm^2)	1×10^{-16}	2.0×10^{-16}	1.5×10^{-16}	1×10^{-17}
D^- (cm^{-3})	1.522×10^{12}	2×10^{15}	2.8×10^{16}	6.78×10^{18}
D^0 (cm^{-3})	1.000×10^{16}	1×10^{15}	1.4×10^{16}	1.60×10^{15}
D^+(cm^{-3})	2.670×10^{18}	2×10^{15}	2.8×10^{16}	1.51×10^{12}
E_D^- (eV)	0.7	0.55	0.46	0.6
E_D^0 (eV)	1.0	0.85	0.76	0.90
E_D^+(eV)	1.3	1.15	1.06	1.20
σ_D (eV)	0.13	0.13	0.13	0.13
σ_N^+, σ_P^- (cm^2)	5×10^{-15}	4×10^{-15}	5.5×10^{-15}	5×10^{-15}
σ_N^0, σ_P^0 (cm^2)	5×10^{-16}	4×10^{-16}	5.5×10^{-16}	5×10^{-16}

The meaning of the symbols are as follows: W is the layer thickness, E_G is the mobility gap, N_C and N_V are the effective density of states in the conduction and valence band respectively, μ_N and μ_P are the electron and hole mobilities, E_D and E_A are the valence and the conduction tail slopes, t_N, t_P are the cross section for electrons and holes in tail states (+, −, 0 indicate the charge status of the tail state), D^-, D^0, and D^+ are the densities of DB enclosed in the three Guassians, E^-, E^0, and E^+ are the peak positions of these Gaussians, σ_D are the standard deviations and σ_N, σ_P are the cross sections for electrons and holes in mid-gap states.

within the values experimentally reported in the literature. The Pool width σ_{DP} was set to reproduce the experimental value of Δ (Eq. (5)) that varies between 0.3 eV and 0.5 eV [9,10]. We split the energy offsets equally between the conduction and the valence band. Neutral boundary conditions (flat bands) were adopted at the front and back contacts. The optical model, accounting for light scattering at rough surfaces conceives the impinging light beam of intensity I as the superposition of N sub-beams of intensity I_j such us $I=\sum_{j=1}^{N} I_J$. Rough interfaces are represented by angles generated by a random seed. At each interface "J" the user can choose the maximum and the minimum angles $\Theta_{MAX,J}$ and $\Theta_{MIN,J}$ (they are inputs of D-AMPS) that the light beams will find at every interface. The random seed generates N different angles Θ_J such us $\Theta_{MIN,J}<\Theta_J<\Theta_{MAX,J}$ and each of the N sub-beams sees a different angle Θ_J. The generation rate $G(x)$ results from adding the generation rates $G_J(x)$ corresponding to each sub-beam, i.e. $G(x)=\sum_{j=1}^{N} G_J(x)$. Roughness is assumed maximum at the TCO/*p* interface (highest values of $\Theta_{MAX,J}$) and slightly decreasing at interfaces closer the back contact. Reflection coefficients are evaluated with the Fresnel equations taking into account the dependence of the refractive indexes with respect to wavelength and with the angle of incidence.

4. Results

Our strategy was first to match the *J–V* and the SR curves of a 500 nm thick a-Si based *p–i–n* using the classical UDM. We repeated the procedure using the different versions of DPM and finally we matched curves of a-Si *p–i–n* devices for other *i*-layer thicknesses.

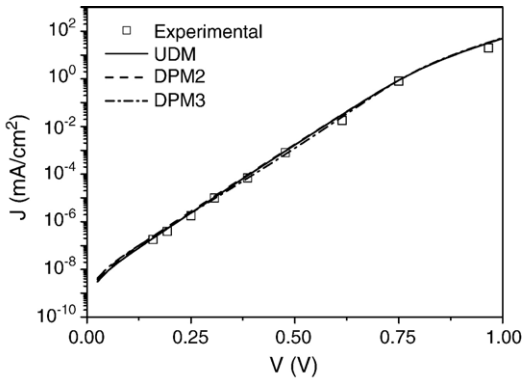

Fig. 1. Fittings of the dark *J–V* curve achieved with D-AMPS using UDM, DPM2 (T_{FR}=460 K), and DPM3. The *i*-layer thickness is 500 nm. The solar cell is in the initial state.

4.1. UDM – 500 nm – initial state

The input parameters resulting from our fittings are listed in Table 1. For the sake of brevity we did not include the buffer layer parameters. The doping densities in the *p*- and *n*-layers were adjusted to reproduce the experimental activation energies. The current at low forward biases and under dark conditions in a-Si *p-i-n* cells is controlled by *i*-layer bulk recombination [23]. In the UDM the recombination at forward voltages is controlled by deep states (DB) at lower biases and by tail states at higher biases. Under illumination tail states control the open circuit voltage (Voc) while mid-gap and tail states together control the fill factor (FF) and the short circuit current (Jsc). The tail cross sections were increased with respect to the values regularly reported in the literature (10^{-15}/10^{-17} cm^2) to narrow the differences between the predicted and the experimental FF and Voc. We could not reach this goal by only increasing the density of mid-gap states in conjunction with their cross sections. The hole mobility was adopted higher than usually (1–2 cm^2 $V^{-1}s^{-1}$) in order to obtain a better match of FF. We strongly needed a mobility gap of 1.72 eV in the *i*-layer to reproduce FF and Voc [15]. Higher values

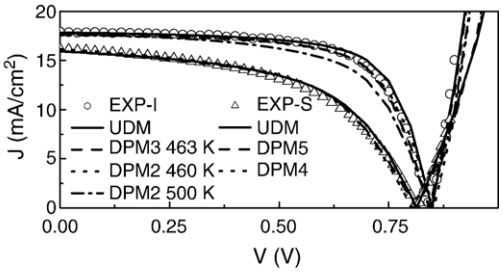

Fig. 2. Fittings of the light *J–V* curve achieved with D-AMPS using UDM, DPM2 (T_{FR}=460 K and 500 K), and DPM3 in the initial state and with UDM, DPM5 (T_{FR}=460 K), and DPM4 in the stabilized state. The *i*-layer thickness is 500 nm.

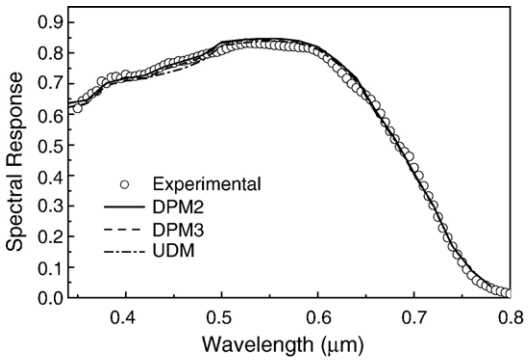

Fig. 3. Fittings of the spectral response curve achieved with D-AMPS using UDM, DPM2 (T_{FR}=460 K), and DPM3. The *i*-layer thickness is 500 nm. The cell is in the initial state.

resulted in an overestimation of Voc. Scattering at rough surfaces was helpful to match the Jsc and the SR at long wavelengths. Defective layers at the *p*/*i* interface or a fixed charge density in the *i*-layer were not necessary. Fittings of the experimental *J*–*V* and SR curves are shown in Figs. 1–3.

4.2. DPM1 – 500 nm – initial state

The second step was to match the same curves with the DPM using the parameters of Table 1 as baseline inputs. The Fermi level was evaluated at $T=T_{FR}$. Assuming $H=3.5\times10^{21}$ cm^{-3}, $U=0.2$ eV, $T_{FR}=500$ K, adopting $E_{DP}=1.15$ eV$=D^+$ (UDM), and σ_{DP} (Eq. (5)) to have $\Delta=E_D+-E_{D^-}*=0.4$ eV [9] (Section 3) the options involving zero or two Si–H bonds ($i=0$ or $i=2$) in the WB → DB reaction gave rise to a very low (< 5×10^{13} cm^{-3}) or to a very high (> 10^{17} cm^{-3}) density of DB in the intrinsic layer bulk resulting in either too optimistic or too pessimistic solar cell efficiencies and in too low or high dark currents respectively. These results forced us to adopt the option $i=1$. This option generates DB densities of ~5×10^{15} cm^{-3} in the *i*-layer bulk. In the DPM recombination and trapping under dark and under illumination conditions becomes much more controlled by DB than in the UDM. The DB profile predicted by the DPM weakens the electric field in the *i*-layer bulk making more difficult the replica of FF especially in thicker *p*–*i*–*n* solar cells. To reduce this undesired effect we decrease the Urbach slope E_{DO} to 45 meV (value that it is within the experimental uncertainty). The DB density predicted by the DPM is highly dependent of E_{DO}. We also increased the electron mobility to 30 cm^2/V/s and introduced a uniform negative density of around 2×10^{15} cm^{-3} in the intrinsic layer to improve our FF and to low our Voc. The density of DB generated by any DPM approach is quite sensitive to the value adopted for E_{DP}. The high density of DB introduced by $E_{DP}=1.15$ eV gave rise to dark currents in excess, poor FF and low Voc. In the literature we find that in intrinsic a-Si the activation energy varies between 0.65 eV and 0.78 eV. The value of E_{DP} of 1.21 eV results in an activation energy of 0.71 eV and decreases the density of DB. Finally to reproduce better FF and Voc we lowered our tail cross sections by a factor of 2.5 and we increased the density of effective states (N_C, N_V) to reduce trapping and recombination further. The DB density in doped layers, where the Fermi level is nearly constant, was adopted uniform but following the exponential dependence with respect to the Fermi level predicted by the DPM [9], i.e.

$$D^+ = D^0\cdot e^{-\frac{2\cdot E_F}{2\cdot E_D(T_{FR})+i\cdot k\cdot T_{FR}}}, D^- = D^0\cdot e^{\frac{2\cdot E_F}{2\cdot E_D(T_{FR})+i\cdot k\cdot T_{FR}}}. \quad (7)$$

The total density of DB is controlled by D^+ (2.63×10^{18} cm^{-3}) in *p*-a-SiC and by D^- in *n*-a-Si (6.78×10^{18} cm^{-3}). The list of input parameters used to fit the *J*–*V* and the SR curves are listed in Table 2. The parameters that remained identical in DPM1 and in UDM were not included (fittings of the dark and light *J*–*V* can be found in Ref. [15]). The matching of the *J*–*V* and the SR characteristic curves with such different models was possible by adopting wider tails and higher tail cross sections in the UDM to compensate the extra trapping and recombination introduced by the DPM near the interfaces.

Table 2
List of input parameters obtained with the different DPM models for the 500 nm thick *p*–*i*–*n* sample

Parameter models used	(*p*) a-SiC	(*i*) a-Si DPM1-I	(*i*) a-Si DPM1-S	(*i*) a-Si DPM2-I	(*i*) a-Si DPM3-I	(*i*) a-Si DPM4-S	(*n*)a-Si
N_c, N_v (cm^{-3})	2×10^{20}	3×10^{20}	3×10^{20}	3×10^{20}	3×10^{20}	3×10^{20}	2×10^{20}
μ_N (cm^2 V^{-1} s^{-1})	10	30	30	30	30	30	20
E_D (meV)	80	45	45	45	45	45	50
f_N^+, f_P^- (cm^2)	1×10^{-14}	6×10^{-15}	6×10^{-15}	9×10^{-15}	9×10^{-15}	6×10^{-15}	1×10^{-15}
f_N^0, f_P^0 (cm^2)	1×10^{-16}	6×10^{-17}	6×10^{-17}	2×10^{-16}	2×10^{-16}	6×10^{-17}	1×10^{-17}
D^- (cm^{-3})	1.53×10^{14}						6.78×10^{18}
D^0 (cm^{-3})	2×10^{16}						2.84×10^{15}
D^+(cm^{-3})	2.63×10^{18}						1.19×10^{12}
σ_N^+, σ_P^- (cm^2)	5×10^{-15}	5×10^{-15}	1×10^{-14}	4×10^{-15}	4×10^{-15}	5×10^{-15}	5×10^{-15}
σ_N^0, σ_P^0 (cm^2)	5×10^{-16}	5×10^{-16}	1×10^{-15}	4×10^{-16}	4×10^{-16}	5×10^{-16}	5×10^{-16}
E_{DP} (eV)		1.21	1.06	1.26	1.16	1.12	
σ_{DP} (eV) (*)		0.153	0.153	–	–	–	
Δ (eV) (*)		0.4	0.4	0.35	0.35	0.5	

The letter I stands for the initial state and the letter S stands for the stabilized state. E_{DP} is the most likely pool energy. Densities D^-, D^0, and D^+ in doped layers are shown only for the DPM1. The highest densities of DB in doped regions (D^+ in *p*-layer and D^- in *n*-layer) are identical in all the DPM models. Δ is the energy separation between the peak of the double occupied D^- and the peak of D^+. (*) These parameters are not independent. They are not inputs of D-AMPS.

4.3. DPM2–DPM3 – 500 nm – initial state

Using the parameters obtained with DPM1 we tried to fit the same curves with DPM2 where directly two Si–H bonds participate in the WB → DB reaction. The modified expression of Powell and Deane is similar to Eq. (3). The term $E_{DO}+ikT/2$ of Eq. (4) is replaced by $2E_{DO}$ making ρ equal to ½ in Eq. (6) [10]. The DB density in the *i*-layer bulk results 3–4 times lower than in DPM1 ($i=2$) [10] but still one order higher than in DPM1 ($i=1$). Hence the predicted dark *J–V* and FF results higher and lower respectively than the experimental values. To reduce trapping and recombination further than in DPM1 we changed the value of Δ from 0.4 eV to 0.5 eV and increased the pool peak E_{PD} from 1.21 eV to 1.26 eV. By doing this we still obtain a reasonable activation energy in the *i*-layer (0.66 eV). Fittings of the light *J–V* and SR curves are shown in Figs. 2–3 (see Ref. [15] for the dark *J–V*). We can see that the predicted FF is still below the experimental figure.

We also explored the matching of *J–V* and SR curves in the initial state with DPM3 ($i=1$) using the DPM1 parameters. The expressions equivalent to the Eqs. (3)–(5) are in DPM3 [11]:

$$N_{DB}(E)=\gamma\left[\frac{2}{F^0_{EQ}(E)}\right]^{\frac{kT_{FR}}{2E_{DO}}}P\left[E+\frac{\sigma^2_{DP}}{2E_{DO}}\right] \quad (8)$$

$$\rho=\left(1+\frac{i\cdot k\cdot T_{FR}}{2\cdot E_{DO}}\right)^{-1} \quad (9)$$

$$\Delta=E_{D^+}-E^*_{D^-}=\frac{\sigma^2_{DP}}{E_{DO}}-U \quad (10)$$

where the coefficient γ has now a more complex expression [11]. In doped layers the equations (Eq. (7)) relating D^+, D^-, D^0 are still valid. Schumm adopts a lower freezing temperature than Powell and Deane: $T_{FR}=463$ K [11]. The decrease of the freezing temperature is accompanied by a decrease of the density of DB predicted by the DPM. Using the DPM1 input parameters (except for σ_{DP}, see Eqs. (5) and (9)) we obtain satisfactory fittings of the *J–V* and SR curves. The input parameters resulting from our fittings are listed in Table 2.

4.4. DPM – 215 nm and 1000 nm – initial state

The next step was to fit light *J–V* curves of a-Si *p–i–n* devices prepared under similar conditions but with different *i*-layer thicknesses. Using the parameters resulting from the 500 nm sample (Table 2) the computed light *J–V* resulted optimistic for the 215 nm sample (overestimation of FF and Voc) and pessimistic for the 1000 nm sample (underestimation of FF and Voc). The predicted dependence of the electric field with respect to the *i*-layer thickness resulted stronger than needed. Similar results were obtained by modeling a-Si *p–i–n* with either the UDM or the DPM. To overcome this problem we allowed for some dispersion in our input parameters. To obtain a reasonable fitting in the 215 nm sample we reduce the value of E_{DP} keeping the *i*-layer activation energy reasonable. We removed the fix negative charge present in the *i*-layer and we slightly increased the cross sections of mid-gap and tail states. Similarly to what happened in the 500 nm thick sample the DPM2 produces more DB than the DPM1. We counterbalanced this effect by increasing E_{DP}. Also as before using the DPM3 we can practically use the same parameters than with DPM1. The resulting input parameters are listed in Table 3. The input parameters needed to achieve the fittings in the 1000 nm sample are also listed in Table 3. In this sample we could not fit the light *J–V* with the DPM2 because it introduces a too high density of DB. Fittings of the light *J–V* curves can be found in Table 1 of Ref. [15].

Table 3
List of input parameters obtained in the initial state with the different DPM models for the 215 nm and for the 1000 nm sample

Parameters (*i*) a-Si	DPM1–215	DPM1–1000	DPM3–215	DPM3–1000	DPM2–215
N_A (cm^{-3})	–	2×10^{15}	–	2×10^{15}	–
μ_N ($cm^2\ V^{-1}\ s^{-1}$)	20	30	20	30	20
μ_P ($cm^2\ V^{-1}\ s^{-1}$)	2	3.5	2	3.5	2
E_D (meV)	45	45	45	45	45
t^+_N, t^-_P (cm^2)	6×10^{-14}	6×10^{-15}	6×10^{-14}	6×10^{-15}	6×10^{-14}
t^0_N, t^0_P (cm^2)	6×10^{-16}	6×10^{-17}	6×10^{-16}	6×10^{-17}	6×10^{-16}
σ^+_N, σ^-_P (cm^2)	1×10^{-14}	5×10^{-15}	1×10^{-14}	5×10^{-15}	1×10^{-14}
σ^0_N, σ^0_P (cm^2)	1×10^{-15}	5×10^{-16}	1×10^{-15}	5×10^{-16}	1×10^{-15}
E_{DP} (eV)	1.16	1.21	1.23	1.21	1.21

4.5. UDM — stabilized state

Using as baseline the parameters obtained in the initial state with UDM we tried to match the light *J–V* curves of a-Si *p–i–n* devices in the stabilized state. The density of DB enclosed by the three Gaussians (D^+, D^0, D^-) were simultaneously increased by the same proportion and the peaks were moved ~90 meV towards the middle of the gap in order to reproduce the increase of the dark activation energy observed in stabilized (*i*)-a-Si [1]. By doing this we increased trapping and recombination losses that in turn increased the dark current and deteriorated the FF. We found out that we could reach an acceptable fitting by either increasing the DB densities or by simultaneously increasing the density of DB and mid-gap state cross sections. We could not fit the light *J–V* curves by only increasing the mid-gap state cross sections keeping the density of DB unaltered. The input parameters resulting from fitting the 500 nm sample are listed in Table 1 and the ones resulting from fitting other thicknesses are listed in Table 2. For the 500 nm thick sample we show our fitting in Fig. 2. Some dispersion in the input parameters was needed to match the three samples with different thicknesses.

4.6. DPM — stabilized state

Assuming that the chemical reactions controlling the defect structure in equilibrium and out of the equilibrium are identical

Schumm derives the following expression for the density of DB in the stabilized state of a-Si [11]:

$$D_{SS}(E) = \gamma \left[\frac{2}{f*^{0}_{E}}\right]^{\frac{k\cdot T_{FR}}{2\cdot E_{DO}}} \cdot P\left(E + \frac{\sigma^{2}_{DP}}{2\cdot E_{DO}}\right) \cdot \left[\frac{n\cdot p}{n_0\cdot p_0}\right]^{\frac{\rho\cdot k\cdot T_{FR}}{2\cdot E_{DO}}} \quad (11)$$

This expression is similar to Eq. (8) but the equilibrium occupation function for neutral states F^{0}_{EQ} is replaced by the non-equilibrium occupation function for neutral states $f*_{E^0}$, and the extra factor $(np / n_o p_o)^B$ is introduced, where n and p are the free carrier concentrations out of equilibrium, n_o and p_o are the same concentrations in equilibrium. The exponent B is given by $B== \rho k T_{FR} / 2E_{DO}$ i.e. it is a function of the freezing temperature (we will recognize the algorithm (11) as the DPM4). Using Eq. (11) and moving the peak energy of the pool E_{DP} closer to mid-gap to approximately fulfill the relationship $E_{DP} \sim E^{o}_{D}$ [11] we reached acceptable fittings adopting Δ equal to 0.35 eV. No changes were needed in the tail state parameters. The electrical parameters resulting from our fittings are listed in Table 2 and the fitting of the light J–V for the 500 nm thick sample is shown in Fig. 2.

An alternative approach to model the stabilize state would be to use DPM1, DPM2 or DPM3 but adopting lower values of E_{DP} than in the initial state to generate more DB on the whole i-layer. In fact the increase of the DB density has to be combined with increasing mid-gap state cross sections to reasonably match the light J–V curves in the stabilized state. In Table 2 we list the parameters obtained for the DPM1. Table 3 lists the input parameters for other thicknesses. We experienced some problems fitting the Voc of the 1000 nm thick solar cell. However the light J–V of this sample shows an anomalously high experimental Voc. (See also Table 1 in Ref. [15]).

5. Discussions

In the defect pool formalism the highest occurrence probability for the WB ↔ DB reaction is reached when two Si–H bonds (i=2) are involved in this reaction but so far this option led us a high density of DB that precluded us from fitting some experimental data (see Section 4). In the DPM3 we have assumed the validity of Eq. (6). However Schumm assumes that the valence band tail slope at the freezing temperatures is equal than at the device operating temperature, i.e. $E_{DO}(T_{FR})=E_{DO}(T)$. This assumption leads to an underestimation of the density of DB. Schumm also adopts a lower freezing temperature than Powell and Deane that also depresses the density of DB. In addition to assume that T_{FR}=463 K and $E_{DO}(T_{FR})=E_{DO}(T)$ Schumm uses cross section for holes that are at least one order lower than the cross sections for electrons. By means of all these assumptions of Schumm we found out that when two Si–H (i=2) participate in the WB ↔ DB reaction trapping and recombination could be reduced to the extend of making possible the fitting of the light J–V of the 500 nm sample (initial and stabilized state) with similar limitations to the ones found with the DPM2. Fig. 4 shows the resulting density of states (the resulting parameters and the fitting of the light J–V are not shown for the sake of brevity). For the sake of comparison we also plot in the same figure the density of states that would have resulted for i=2 if the parameters of Table 2 (corresponding to i=1), where we have T_{FR}=500 K and $E_{DO}(T_{FR}) \neq E_{DO}(T)$, would have been used (the density DB for i=1 was plot in Fig. 2 of Ref. [15]). This high density of DB does not allow us to reproduce the J–V curves in the initial state. Adopting Schumm's cross sections, the highest as possible values of E_{DP} and increasing the hole mobility over 7 cm^2 V^{-1} s^{-1} we could not match either our data with the DPM1 adopting i=2. We concluded one more time that the option i=2 in the DPM1 is not appropriate for solar cell modeling. The option i=2 in the DPM3 has the weak point of not correcting the valence band tail with temperature. On the top of that the light J–V of the 1000 nm sample could not be matched with the DPM3 even far from Voc. Hence a different approach is needed to allow for two Si–H in the WB ↔ DB reaction.

The DPM2 directly assumes that two Si–H bonds are involved in the WB ↔ DB reaction and it introduces the concept

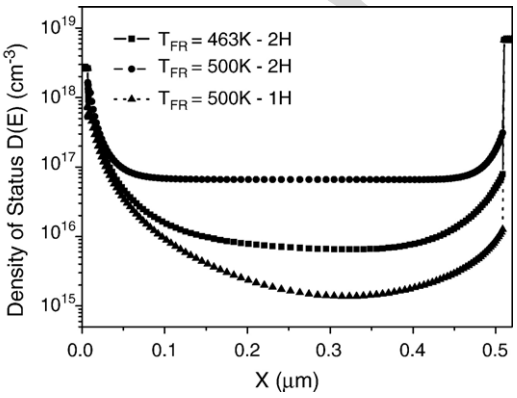

Fig. 4. Comparison of the DB densities obtained with the DPM3 algorithm when one or two Si–H bonds are participating in the WB ↔ DB reaction. For one Si–H we assume a temperature dependent Urbach tail, T_{FR}=500 K and we use our parameters of Table 2, (7). For two Si–H we plot the equivalent DB density (!), and we also assume a temperature independent Urbach tail, T_{FR}=463 K and we adopt Schumm's parameters [11] (,). The i-layer thickness is 500 nm. The cell is in the initial state.

Table 4
List of input parameters obtained with the DPM2–DPM5 models (i=2) for the 500 nm sample

Parameters (i) a-Si	DPM2–215 T_{FR}=460 K(I)	DPM2–500 T_{FR}=460 K(I)	DPM5–500 T_{FR}=460 K (S)	DPM2–1000 T_{FR}=460 K(I)
μ_N (cm^2 V^{-1} s^{-1})	30	30	30	30
μ_P (cm^2 V^{-1} s^{-1})	3.5	5.0	3.5	5.0
E_D (meV)	45	45	45	45
t^{+}_{N}, t^{-}_{P} (cm^2)	6×10^{-14}	9×10^{-15}	9×10^{-15}	6×10^{-15}
t^{0}_{N}, t^{0}_{P} (cm^2)	6×10^{-16}	2.0×10^{-16}	2.0×10^{-16}	1.5×10^{-16}
σ^{+}_{N}(cm^2)	2.5×10^{-14}	4×10^{-15}	4×10^{-15}	1×10^{-15}
σ^{0}_{N} (cm^2)	2.5×10^{-15}	4×10^{-16}	4×10^{-16}	1×10^{-16}
σ^{-}_{P} (cm^2)	2.5×10^{-14}	4×10^{-15}	4×10^{-15}	1×10^{-15}
σ^{0}_{P} (cm^2)	2.5×10^{-15}	4×10^{-16}	4×10^{-16}	1×10^{-16}
E_{DP}(eV)	1.26	1.26	1.15	1.28
Δ(eV)	0.35	0.35	0.35	0.35

(I) stands for the initial state and (S) for the stabilized state.

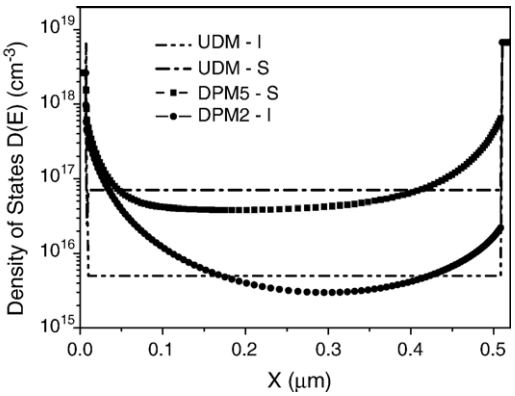

Fig. 5. The DB density obtained in the initial (and stabilized) state with the DPM2 (DPM5). The freezing temperature is 460 K and the *i*-layer thickness is 500 nm. The DB densities obtained with the UDM are shown for the sake of comparison.

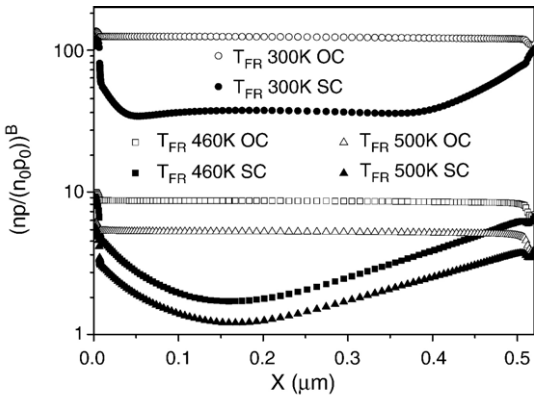

Fig. 6. Factor $(np/n_op_o)^B$ at room temperature, at $T=T_{FR}=460$ K and at $T=500$ K. The factor is evaluated at short circuit (SC) and at open circuit voltage (OV) conditions. The defect pool model is DPM5 and the *i*-layer thickness is 500 nm.

of the hydrogen density of states. However we encountered difficulties in reproducing the FF of the 500 nm sample and we could not match the light *J–V* of the 1000 nm sample. Following the idea of Schumm [11] we adopted a lower freezing temperature within the range reported in the literature [24]. We found that by lowering the freezing temperature to $T_{FR}\sim460$ K and by slightly increasing (decreasing) the hole mobility (the DB cross sections) (see Table 4) we could reproduce the experimental FF of the 500 nm sample in the initial state without loosing the match of the dark *J–V* and of the SR curves. Lower values of the freezing temperature would allow to leave the hole mobility and the cross sections unchanged ($T_{FR}\sim440$ K). Our results for $T_{FR}\sim460$ K are shown in Figs. 1–3 and the density of DB is plotted in Fig. 5. Using this freezing temperature the matching of the light *J–V* of the 1000 nm sample and the removal the negatively ionized charge added in the intrinsic layer (Section 4.2) became also possible. The input parameters used to fit the solar cell characteristics are listed in Table 4 and the resulting Jsc, FF, and Voc are shown in Table 5.

Powell and Deane (PD) did not explicitly discuss the stabilized state of a-Si. For the stabilized state we included in the algorithm derived by Powell and Deane the modifications suggested in Eq. (11) by Schumm [11], i.e. we included the extra factor $(np/n_op_o)^B$ and we replaced the equilibrium occupation function F^0_{EQ} by the non-equilibrium function $f^*_{E^0}$. The resulting light *J–V* curves are shown in Fig. 2 (500 nm sample) and in Table 5. The input parameters are listed in Table 4. Similar results were obtained for the 215 nm and the 1000 nm samples (see Tables 4 and 5). A dispersion in the input parameters was again needed to match the light *J–V* for different *i*-layer thicknesses. In Fig. 5 we show the DB density resulting in the stabilized state. We recognize this modification of the PD algorithm as the DPM5 model. Comparing the densities of DBs predicted with DPM2 and with DPM5 we can see that the stabilized density of DB also increases exponentially towards both the interfaces but results more flat in the bulk. In the annealed state the shape of the DB densities is highly dictated by the occupation function for neutral states F^0_{EQ} and by the value of E_{DP} (the most likely energy where DB are formed). The occupation function F^0_{EQ} reaches its minimum values (and $D(E)$ its maximum) at the interfaces. Due to the fact that E_{DP} should be adopted above mid-gap the defect pool model creates more DB near the *p*/*i* interface than near the *i*/*n* interface. In the hypothetical situation where E_{DP} would be placed below mid-gap more states would be created near the *i*/*n* interface. In the stabilized state the function $f^*_{E^0}$, that it is much more homogeneous than F^0_{EQ} in the intrinsic layer, tends to flat the density of DB in the bulk and to depress the same density near the interfaces being its effect more pronounced at the *p*/*i* interface where the majority carrier concentration (holes) is more affected by the presence of light. On the other hand the factor $(np/n_op_o)^B$, that it is plotted in Fig. 6, tends to increase the density of DB almost uniformly on the whole intrinsic layer.

Using the input parameters listed in Table 4 we plot in Fig. 7 the light *J–V* curves that would have resulted from assuming that the light soaking experiment was performed at short circuit conditions (OC), at the maximum power point (MPP) and at Voc (OC). These light *J–V* curves were generated using the electrical parameters resulting from fitting the experimental light *J–V* obtained by light soaking the solar cell at open circuit

Table 5
Fitting of the light *J–V* curves with the DPM2–DPM5 models lowering the freezing temperature to 460 K

	Experimental (I–S) 215 nm	DPM2–5 (I–S) 215 nm	Experimental (I–S) 500 nm	DPM2–5 (I–S) 500 nm	Experimental (I–S) 1000 nm	DPM2–5 (I–S) 1000 nm
FF	0.640–0.533	0.655–0.537	0.68–0.52	0.670–0.548	0.595–0.422	0.567–0.450
Voc (V)	0.815–0.797	0.811–0.776	0.84–0.81	0.852–0.812	0.818–0.840	0.871–0.797
Jsc ($mAcm^{-2}$)	14.77–13.74	14.70–14.00	17.95–16.22	17.73–15.95	19.08–15.22	18.93–14.94

The letter I corresponds to the initial state and the letter S to the stabilized state.

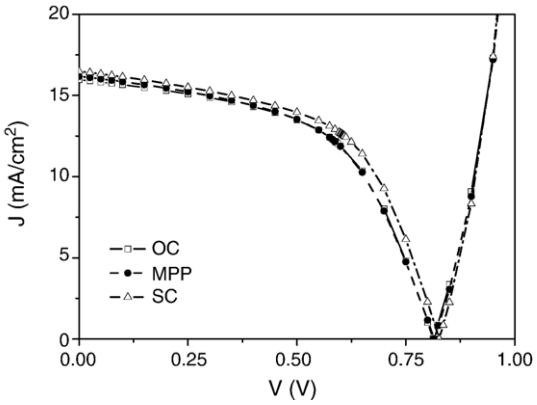

Fig. 7. Light J–V predicted with DPM5 for the 500 nm thick solar cell in the stabilized state light soaking the sample at short circuit (SC), at maximum power point (MPP) and at open circuit voltage (OC) conditions. The input parameters are taken from fitting the light J–V at OC conditions.

conditions but using the free carrier concentrations of the 500 nm sample corresponding to the SC, the MPP, and the OC conditions. We can see that the algorithm proposed by Schumm (and the one of the DPM5) is sensitive to the sample history being its sensitivity higher for lower freezing temperatures as it can be seen in Fig. 6. The defect pool model assumes that the DB density remains frozen below T_{FR}. Hence the DB density of Eqs. (3), (8), and (11) must always be evaluated at $T=T_{FR}$! In particular in the algorithm proposed by Schumm for the a-Si stabilized state this statement implies that the free carrier concentrations in the factor $(np / n_o p_o)^B$ (Eq. (11)) correspond to a device working at the temperature $T=T_{FR}$. In Fig. 6 we plot this factor $(np / n_o p_o)^B$ at room temperature, at $T=T_{FR}$ and at $T=500$ K. If these concentrations would have been calculated at room temperature the algorithm of DPM5 would have predicted an unreasonable high density of DB in the stabilized state and an extremely poor FF in the solar cell that would have made impossible the fitting of the experimental light J–V.

Using the DPM2 and DPM5 models we have also obtained a reasonable dependence of the dark J–V curve with respect to the intrinsic layer thickness and we could reproduce the increase of the low forward dark J–V and the decrease of the high-forward dark J–V experimentally observed after light soaking [25] but we will discuss these issues in future publications.

6. Conclusions

The experimental J–V and SR characteristic curves of a-Si p–i–n solar cells could be matched by either assuming a uniform density of dangling bonds (UDM) or by using the defect pool model (DPM). In the DPM the option of two Si–H bonds participating in the weak-dangling bond reaction results in quite high densities of dangling bonds that make very difficult the reproduction of the fill factor especially in thick samples. However by adopting a lower freezing temperature (460 K instead of 500 K) in the second algorithm published by Powell and Deane, where two Si–H bonds participate in the creation of dangling bonds, the fitting of solar cell characteristic curves becomes possible for any intrinsic layer thickness. The second version published by Powell and Deane seems the most appropriate for a-Si based solar cell modeling in the annealed state and it can be conveniently adapted to the stabilized state using the ideas proposed by Schumm. The density of dangling bonds in the stabilized state results nearly flat in the intrinsic layer bulk and in absolute terms increases more significantly near the interfaces. The algorithm proposed by Schumm is sensitive to the sample history. We have compared the values of the electrical input parameters resulting from matching the experimental curves of a-Si p–i–n solar cells with the different versions of the defect pool model published in the literature.

Acknowledgments

The authors highly appreciate the financial support of Agencia Nacional para la Promoción de la Ciencia y la Tecnología (PICT 11–12523). They also would like to express their gratitude to the team conducted by R.E.I. Schroop and J.K. Rath of SID-Physics of Devices Utrecht University, Debye Institute for providing the experimental data. We would like to specially thank Dr. J.K. Rath for useful discussions.

References

[1] R. Schropp, M. Zeman, Amorphous and Microcrystalline Silicon Solar Cells, Modeling, Materials and Device Technology, Kluwer Academic Publishers, Boston, 1998.
[2] H. Tasaki, W. Kim, M. Hallerdt, M. Konagai, K. Takahashi, J. Appl. Phys. 63 (1988) 550.
[3] S. Nag, J. Nicque, C. Malone, J. Arch, D. Heller, S. Fonash, C. Wronski, Sol. Energy Mater. 28 (1992) 285.
[4] P. Chatterjee, J. Appl. Phys. 76 (1994) 1301.
[5] X. Li, S. Wagner, M. Bennett, J. Hou, F. Rubinelli, S. Fonash, Montreux, Switzerland, October 12–16, Proc. 11th European Photovoltaic Sol. Energy Conf., 1993, p. 703.
[6] M. Block, J. Non-Cryst. Solids 166 (1993) 701.
[7] H. Branz, R. Crandall, Sol. Cells 27 (1989) 159.
[8] K. Winer, Phys. Rev., B 41 (1990) 12150.
[9] M. Powell, S. Deane, Phys. Rev., B 48 (1993) 10815.
[10] M. Powell, S. Deane, Phys. Rev., B 53 (1996) 10121.
[11] G. Schumm, Phys. Rev., B 49 (1994) 2427.
[12] M. Stutzmann, Philos. Mag., B 56 (1987) 63.
[13] M. Stutzmann, Philos. Mag. Lett. 66 (1992) 147.
[14] F. Rubinelli, R. Jiménez, J. Rath, R. Schropp, J. Appl. Phys. 91 (2002) 2409.
[15] E. Klimovsky, J. Rath, R. Schropp, F. Rubinelli, J. Non-Cryst. Solids 338–340 (2004) 686.
[16] S. Guha, J. Yang, A. Pawlikiewicz, T. Glatfelter, R. Ross, S. Ovshinsky, Appl. Phys. Lett. 54 (1989) 2330.
[17] R. Jiménez, F. Rubinelli, J. Rath, R. Schropp, J. Non Cryst. Solids 299–302 (2002) 1131.
[18] R. Jiménez, F. Rubinelli, W.M. Arnoldbik, J. Rath, R. Schropp, Sol. Energy Mater. Sol. Cells 81 (2004) 73.
[19] G. Schumm, Appl. Phys. Lett. 66 (1995) 2706.
[20] M. Zeman, G. Tao, M. Trijssenaar, J. Willemen, W. Metselaar, R. Schropp, Mater. Res. Soc. Proc. 377 (1995) 639.
[21] M. Powell, R. Wehrspohn, S. Deane, J. Non Cryst. Solids 299–302 (2002) 556.
[22] F. Rubinelli, J. Rath, R. Schropp, J. Appl. Phys. 89 (2001) 4010.
[23] F. Rubinelli, J. Arch, S. Fonash, J. Appl. Phys. 72 (1992) 1621.
[24] R. Street, in: R. Chan, E. Davis, M. Ward (Eds.), Hydrogenated Amorphous Silicon, Cambridge University Press, 1991, p. 172.
[25] B. Rech, C. Beneking, S. Wieder, H. Wagner, Proc. 14th European Photovoltaic Sol. Energy Conf., Barcelona, Spain, 1997, p. 2089.